AIAA 81-4185

Experimental Substantiation for Hovering Rotor Vertical Impedance Calculations

Kanichiro Kato* and Takashi Yamane†
University of Tokyo, Tokyo, Japan
and
Tomoari Nagashima,* Naohiro Iboshi,‡ and Kazuhiro Yamagishi§
National Defense Academy, Yokosuka, Japan

An experiment using a model rotor was conducted to ascertain the accuracy of theoretical impedance calculations. A two-bladed balsa rotor of 1.2 m diam was constructed with a force-sensing device integrated within the hub. The apparatus was so designed that the rotor could perform forced vertical oscillations of varying frequencies, and the resulting hub vertical loads were measured in the nonrotating frame. The conclusions obtained after correlation of the measured and theoretical results were that the quasisteady aerodynamic assumption determines only the rough trend of these impedance characteristics and that a typical section aerodynamic analysis using Loewy's lift deficiency function can predict impedance peaks and clefts occurring near the multiples of the blade passage frequencies due to the preceding and returning wakes.

Introduction

THE analytic development of accurate frequency domain rotor impedances is desirable because the process allows the separate treatment of the rotor and airframe.

The research in this field is new and adequate analytical methods have not been established. In addition, little experimental data exist for the verification of theoretical analyses. To the best of the authors' knowledge, Refs. 1-12 are the main contributions in this field. Cansdale et al.[1-3] proposed techniques of measuring impedances of model rotors. Kuczynski[4] has shown measured hub-moment impedances and correlations with theoretical analyses of a hingeless rotor. Peters and Ormiston[5] have formulated an impedance calculation procedure using a generalized harmonic balance method which takes blade flapwise deformations into account. One of the interesting results of Peters work[6] is that the hub moment vs hub angle frequency response in hover (as obtained from Ref. 4) correlated with the theoretical analysis. Hohenemser and Yin[7] have proposed another impedance calculation procedure with a finite blade element method for hub moment impedances. Yen and McLarty[8] discussed the methods currently used in the coupled-rotor/fuselage analyses. Warmbrodt and Friedmann[9] have formulated the coupled-rotor/rigid-fuselage equations of motion.

Kato and Yamane[10-12] have proposed a procedure for impedance calculations and numerically predicted some typical impedance characteristics. Their formulations allow for the blade's flapwise and chordwise bending as well as torsional deformations and give impedances (including simultaneously those from interharmonic coupling) for hub excitations of arbitrary frequencies. The most restrictive assumptions of their formulations were that the quasisteady aerodynamic loads were used and integrated by strip theory.

This paper presents an experimental study of a model rotor with related theoretical calculations as a preliminary investigation conducted to verify the theory discussed in Ref. 10 of the formulation of the hover impedance calculations.

This paper compares the measured hub vertical loads due to hub plunging with those predicted by the theory. This impedance was selected because it is equally affected by airloads, inertial loads, and blade elastic deformations. The measured impedance covers a forcing frequency range of $\omega/\Omega \cong 0.5 \sim 6$, where ω and Ω denote the hub forcing frequency and rotor rotational speed, respectively. The model blades were made of balsa in order to minimize the inertial loads relative to the airloads and to facilitate the accurate airload measurements. Two approaches were taken in the theoretical impedance calculations concerning the lift deficiency function $C(k)$, where k is the reduced frequency. One approach is to use the quasisteady assumption, $C(k) = 1.0$, as proposed in Ref. 10. The other is to use the lift deficiency function $C'(k,m,h)$ derived by Loewy in Ref. 13, where m and h denote the forcing frequency nondimensionalized by the rotor speed (ω/Ω) and the wake spacing nondimensionalized by the semichord, respectively. The latter approach, which has been used in blade flutter analyses (e.g., Refs. 14 and 15), results in better correlations for these model rotor tests.

Apparatus and Instrumentation

The general view of the apparatus is shown in Fig. 1. The details of the hub assembly are shown in Figs. 2 and 3. The rotor shaft was forced to oscillate vertically from the upper end, while driven through a torque coupling from the lower end. The upper end was supported by a nonrotating, perforated, thin (1.0 mm thick) Duralumin plate using a miniature bearing housing. Eight bonded strain gages on both plate surfaces were used to detect dynamic loads. The lower end of the rotor shaft was fixed to the torque coupling and consisted of a grooved circular plate (0.2 mm thick) made of phosphorous bronze which allowed the rotating hub to plunge vertically while supplied with rotating torque. The hub displacements were measured by a differential transducer as shown in Fig. 3.

The blade was made of lacquer-coated balsa with a radius of 600 mm and a chord of 80 mm, with a uniform section from root to tip. The blade was rigidly connected (without hinge) to the shaft. The blade pitch angle was preset collectively with a pitch change attachment.

Received Feb. 13, 1980; revision received Aug. 11, 1980.

*Professor, Department of Aeronautics.
†Graduate Student (presently with Mechanical Engineering Laboratory).
‡Assistant, Department of Aeronautics.
§Graduate Student, Department of Aeronautics.

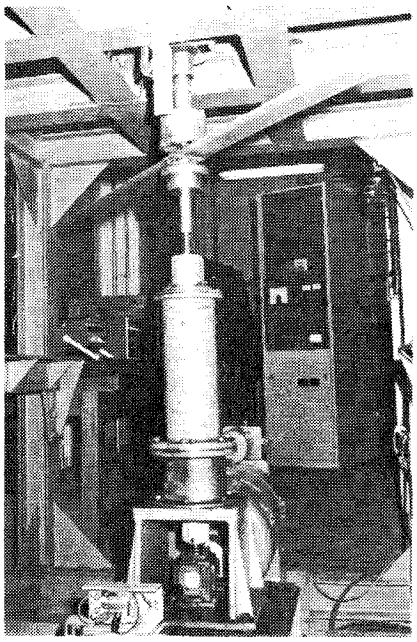

Fig. 1 General view of the apparatus.

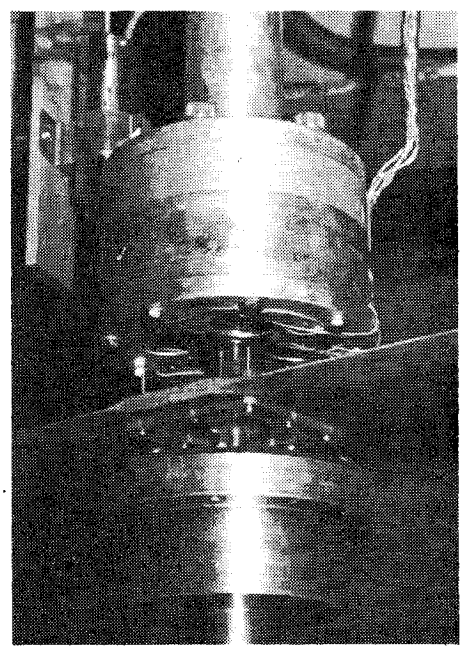

Fig. 2 Model rotor hub assembly.

The model rotor had two blades with the solidity and Lock number being 0.085 and 20.0, respectively. The weight of each was 37.4 g. The elastic axis coincided with the cross-sectional center of gravity which was located at 50% chord. The nonrotating natural frequencies for the first flapwise-bending and torsion of the blade were 12 and 91 Hz, respectively. The mass and the elastic properties are summarized in Table 1. There were slight differences between the two blades and the averages of the two were used in the theoretical analyses.

The blade section is noted as A-A in Fig. 3, with a maximum thickness of 6.0 mm. This airfoil was adopted for ease of maintaining the shaping accuracies and because a sharp leading edge improves the section characteristics at low Reynolds number. The static aerodynamic characteristics, obtained at Reynolds number of 1.06×10^5, are shown in Fig. 4. For comparison Fig. 4 shows the characteristics of NACA 0012 airfoil with a trip wire near the leading edge, measured at Reynolds number of 0.58×10^5. The model blade was

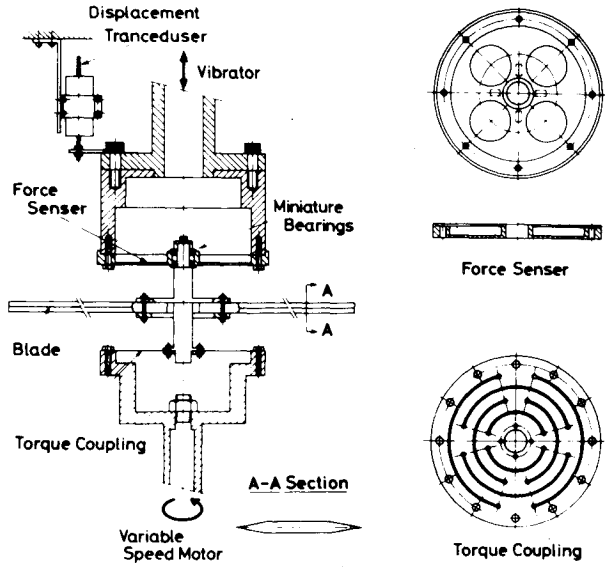

Fig. 3 Hub assembly.

Table 1 Model blade mass and elastic properties

Property	Blade 1	Blade 2
Flapwise bending stiffness, $kg\cdot m^2$	0.333	0.340
Chordwise bending stiffness, $kg\cdot m^2$	44.0	44.0
Torsional stiffness, $kg\cdot m^2/rad$	0.0844	0.0867
Weight per blade, kg	3.74×10^{-2}	3.75×10^{-2}
Mass per unit span, $kg\cdot s^2/m^2$	6.36×10^{-3}	6.38×10^{-3}
Moment of inertia per unit span, $kg\cdot s^2$	2.12×10^{-6}	2.13×10^{-6}

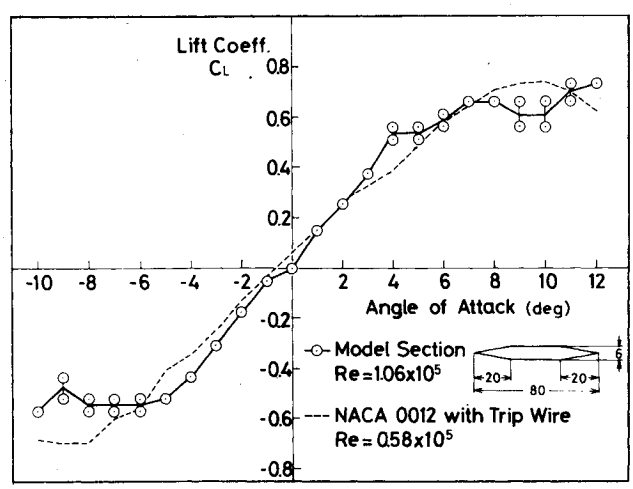

Fig. 4 Static characteristics of the model blade section.

operated at the typical Reynolds number of 10^5 and the cross section was assumed to have a lift curve slope of 2π within an angle-of-attack range of ±5 deg. The angle-of-attack variations during forced oscillations were within about ±1 deg at the blade tip.

The measurements of the hub displacements and loads were amplified and recorded on a data recorder. After digitizing, these signals were fed into a fast Fourier transform (FFT) processor through an antialiasing filter to obtain the averaged amplitude and phase spectra. These measurements were iterated with changing hub forcing frequencies. The above procedure was repeated with and without rotor blades. The

Table 2 Summary of experimental conditions

Pitch angle,[a] θ, deg	Rotor speed, Ω, rpm	Air density, ρ, kg·s^2/m^4	Steady thrust,[b] C_T	Wake spacing,[c] h
0.0	306	0.117	0	0.0
0.0	405	0.117	0	0.0
2.9	312	0.117	0.830×10^{-3}	0.96
2.9	404	0.117	0.918×10^{-3}	1.01
5.0	306	0.118	2.55×10^{-3}	1.68
5.0	401	0.118	2.73×10^{-3}	1.74

[a] Root pitch angle is shown. Torsional deformation possibly increases pitch angle.
[b] $C_T = T/[\rho\pi R^2(\Omega R)^2]$, where T is thrust measured and R rotor radius.
[c] $h = 4\sqrt{C_T/2}/\sigma$, where σ is rotor solidity and C_T is based on measurement.

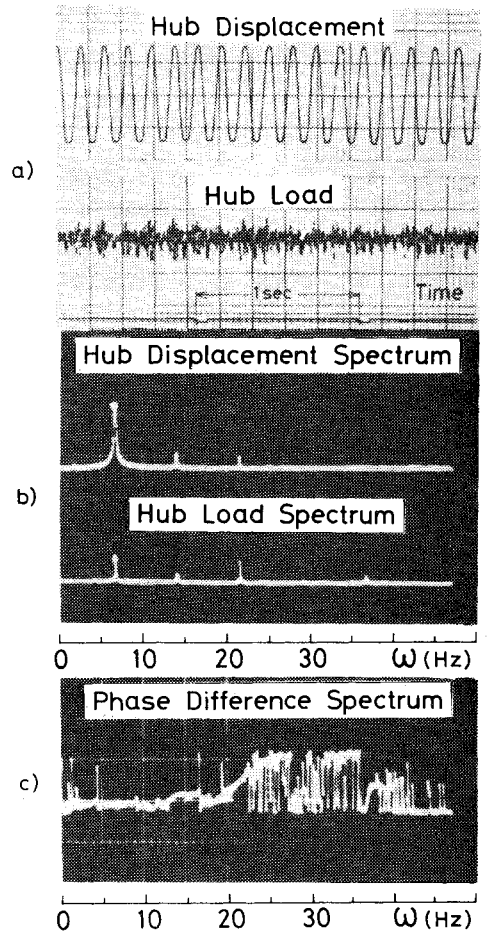

Fig. 5 Sample data reduction ($\omega = 6.9$ Hz, $\Omega = 400$ rpm, $\theta = 0$ deg, without blades).

data with rotor blades installed were taken first and used to determine the impedance of the whole apparatus Z_T, the impedance of the rotor with rig. A similar test was then repeated without the rotor blades to define the rig impedance Z_0. The rotor impedance Z_B can be obtained as the vector subtraction of $Z_T - Z_0$.

Experimental Results

Impedances were measured at six different rotor operating conditions: the combinations of the two rotor speeds ($\Omega \cong 300$ and 400 rpm) and three blade pitch settings ($\theta \cong 0$, 3, and 5 deg). These conditions are summarized in Table 2 with the thrust coefficients C_T measured and the wake spacings h estimated assuming a rigid wake:

$$h = \frac{2\pi u}{bQ\Omega} = \frac{4}{\sigma}\sqrt{\frac{C_T}{2}} \qquad (1)$$

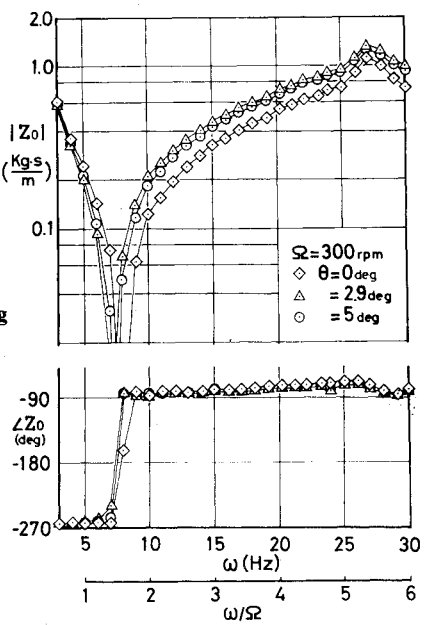

Fig. 6 Measured rig impedances.

where, according to Loewy's notations, u, b, Q, and σ denote downwash at the rotor disk ($\Omega R\sqrt{C_T/2}$), semichord, number of blades, and rotor solidity ($2bQ/\pi R$), respectively. The hub forcing frequency ω was varied between 3-30 Hz. The maximum hub displacement and the maximum hub load were about ± 1 mm and ± 0.1 kg, respectively. The signal-to-noise ratio was more than 10 except for $\omega/\Omega \cong 1$, where noise meant the background levels of oscillatory hub forces without forced oscillatory displacements and it consisted of mainly 1/rev (1Ω) frequency components. The reduced frequency k was about 0.1 for $\omega/\Omega = 1.0$ at 75% radius. The Reynolds number was $0.7 \sim 1.0 \times 10^5$ at 75% radius for the rotor speed of $\Omega = 300 \sim 400$ rpm.

An example of the data reductions is shown in Fig. 5 for a forcing frequency of $\omega = 6.9$ Hz and a rotor speed of $\Omega = 400$ rpm. Figure 5a shows the records of the hub displacement (upper row) and the hub load (lower row), the abscissa being time. Figure 5b presents the spectra of the displacement (upper row) and the load (lower row), while Fig. 5c gives the phase difference between the hub load and the displacement, respectively, both of the abscissas being the hub forcing frequency ω in Hz. As shown in the figure, the input (hub displacement) is not necessarily an exact sinusoidal wave. There are some harmonic contents (other than the forcing frequency) in the load response which are probably due to the noises from the bearing support. These undesirable harmonics can be eliminated without interference through a digitized FFT processor and have negligible effect on the measured impedance in hover. The measured results are shown in Figs. 6-9.

Figure 6 shows the rig impedance Z_0 (impedance without blades) for three pitch settings. This impedance was affected little by the rotor speeds and has a natural frequency of ap-

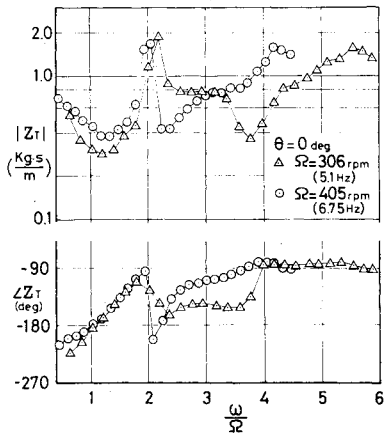

Fig. 7 Measured rotor impedances with rig ($\theta = 0$ deg).

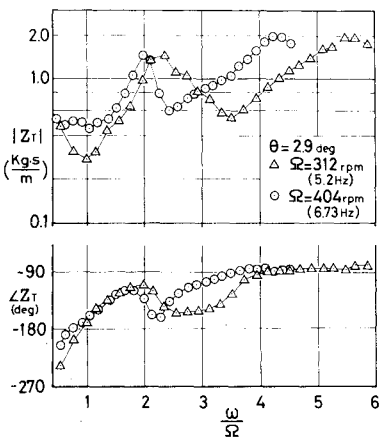

Fig. 8 Measured rotor impedances with rig ($\theta = 2.9$ deg).

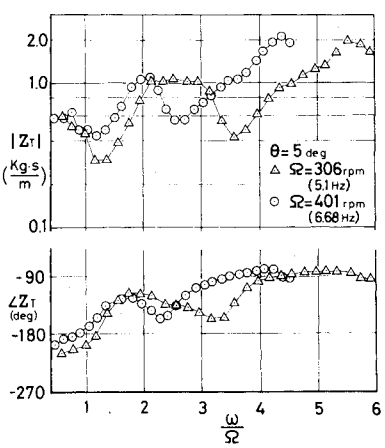

Fig. 9 Measured rotor impedances with rig ($\theta = 5$ deg).

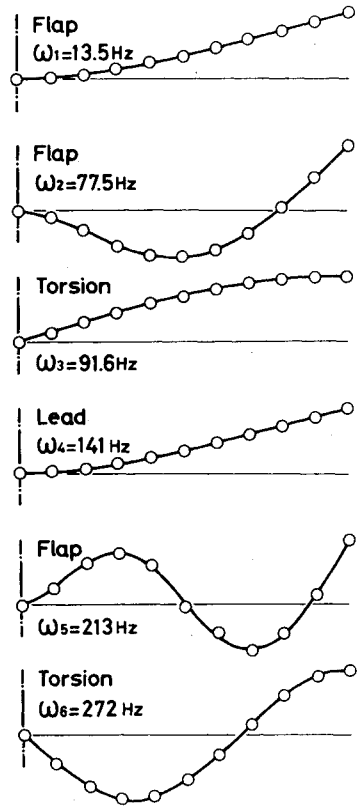

Fig. 10 Model blade modal characteristics ($\theta = 0$ deg).

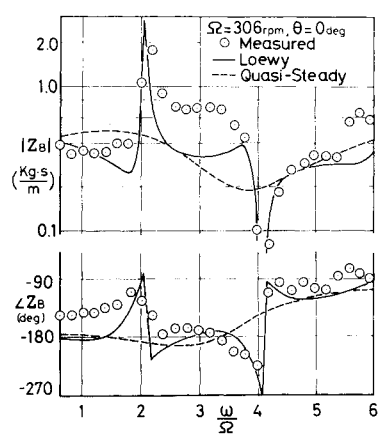

Fig. 11 Measured and calculated rotor impedance ($\Omega = 306$ rpm, $\theta = 0$ deg).

proximately 8 Hz, which was carefully separated from the first flap-bending natural frequency of the blade. The differences of the three rig impedances are due to the mass of the pitch-change attachment: different attachments were used, the mass being 13.7 g for 3 deg and 9.8 g for 5 deg.

Figures 7-9 show the measured impedances of the whole apparatus Z_T (rig plus rotor) for three pitch settings of 0, 3, and 5 deg, respectively, the rotor speed Ω being taken as a parameter. The upper and lower ordinates are the amplitude and the phase of Z_T, respectively, while both the abscissas are the normalized hub forcing frequency ω/Ω. It should be noted that in Fig. 7 ($\theta = 0$ deg) there are precipitous peaks and clefts in the amplitude plots at $\omega \cong 2\Omega$ and 4Ω, respectively. These peaks and clefts become less remarkable as the pitch setting angle increases. It is these peaks and clefts that manifest the effect of the shed vortices from the preceding blade as is shown below. Throughout the tests, the measurements were repeatable within the 10% deviations from the mean in terms of impedances.

Correlation with Theory

The theoretical impedance calculations were conducted according to the procedure given in Ref. 10. The blade deformations were composed by the six uncoupled modes. Actually, two sets of them were used according to the rotor speeds used ($\Omega = 300$ and 400 rpm) in the experiment; using the properties shown in Table 1, natural modes were calculated for the two typical rotor speeds, $\Omega = 308$ and 403 rpm, with zero pitch setting and were used even for the cases with nonzero pitch settings. Figure 10 is the sample result of the modal analysis conducted at $\Omega = 308$ rpm, where ω_1 through ω_6 are the natural frequencies of each mode. It should be noted that formulations of the Ref. 10 can be used for the hingeless rotors by replacing the two rigid (flap and lag) modes with the first two flapwise and chordwise bending modes.

The comparisons between the calculated and measured impedances are shown in Figs. 11-16 for the six different operating conditions. The rotor speed Ω and the pitch setting θ

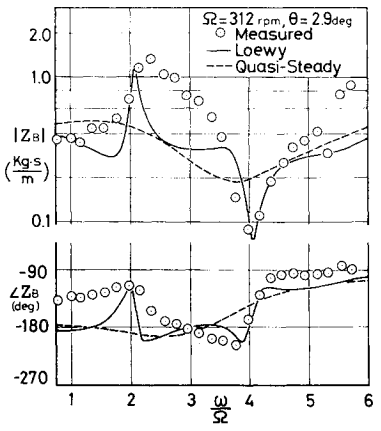

Fig. 12 Measured and calculated rotor impedance ($\Omega = 312$ rpm, $\theta = 2.9$ deg).

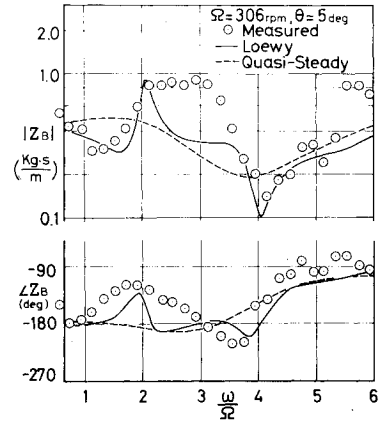

Fig. 13 Measured and calculated rotor impedance ($\Omega = 306$ rpm, $\theta = 5$ deg).

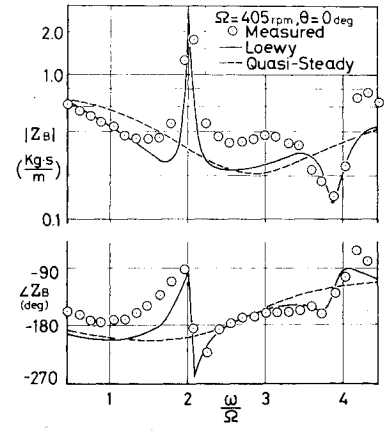

Fig. 14 Measured and calculated rotor impedance ($\Omega = 405$ rpm, $\theta = 0$ deg).

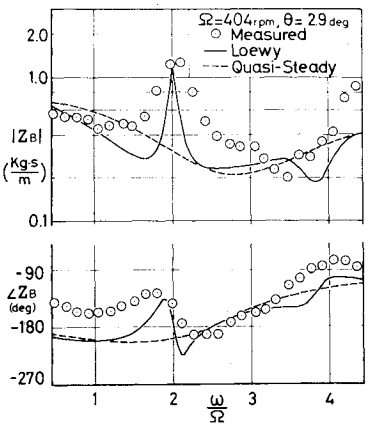

Fig. 15 Measured and calculated rotor impedance ($\Omega = 404$ rpm, $\theta = 2.9$ deg).

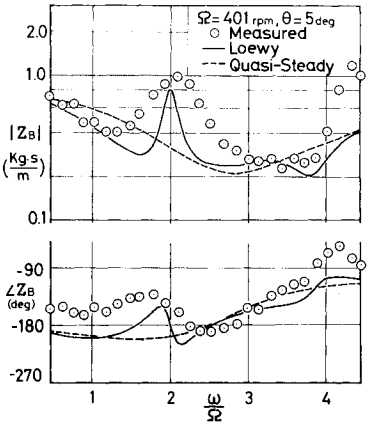

Fig. 16 Measured and calculated rotor impedance ($\Omega = 401$ rpm, $\theta = 5$ deg).

are shown in the upper right corner of each figure. The upper and lower ordinates are the amplitude and the phase of the rotor impedance Z_B (without rig), respectively, while the abscissa is the normalized hub forcing frequency ω/Ω.

The quasisteady theory results shown neglect all the effects of preceding and returning wakes [$C(k) = 1.0$]. In the Loewy analysis shown, the lift deficiency function, $C'(k,m,h)$, was calculated at 75% span and this typical value was applied to all the other sections. This approach reflects approximately the effect of the shed vortices of the preceding and returning wakes. When calculating $C'(k,m,h)$, the wake spacing h was obtained from Eq. (1), where C_T was based on the measured value as shown in Table 2.

The analysis with the Loewy's function agrees fairly well with the amplitude peaks and clefts which appear near the multiples of the blade passage frequency $Q\Omega$, where Q is the number of blades. They are the effect of the preceding shed wakes, and become most predominant at the zero pitch setting. Also, the quasisteady assumption is unable to show such wake effects, although it could predict rough impedance trends for the wide forcing frequency ranges.

The most uncertain portion of this experimental study was the unsteady aerodynamic characteristics of the model blade section; no data were available for this blade oscillating at the Reynolds number around 10^5. The measured results seemed to be less correlated with theory at the rotor speed of $\Omega \cong 300$ rpm than at $\Omega \cong 400$ rpm. This might be due to the unsteady aerodynamic section characteristics at the low Reynolds numbers.

Conclusion

The vertical loads due to hub plunging were measured by a model rotor and compared with the theory of Ref. 10. The correlation study between the theory and the test showed clearly the existence of the interferences between the blade airloads and the preceding wakes, so far as this particular model rotor experiment was concerned. The interference phenomenon becomes most prominent at near-zero collective pitch, as Loewy correctly pointed out.[13]

The effect of the preceding shed vortices appears only in the relatively narrow frequency ranges near the multiples of blade passage frequency and, except for those narrow areas, the quasisteady airload theory could predict the rough trend of this impedance. Actually the wake effect may not be so obvious because the wake spacings are larger in practical rotors.

References

[1] Cansdale, R., Gaukroger, D. R., and Skingle, C. W., "A Technique for Measuring Impedances of a Spinning Model Rotor," Royal Aircraft Establishment TR-71092, 1971.

[2]Cansdale, R. and Gaukroger, D. R., "Impedance Measurements on a Spinning Model Helicopter Rotor," Aeronautical Research Committee CP-1389, July 1976.

[3]Gaukroger, D. R. and Cansdale, R., "Rotor Impedance Measurements at Model Scale," *Vertica,* Vol. 1, No. 1, 1976, pp. 55-66.

[4]Kuczynski, W. A., "Experimental Hingeless Rotor Characteristics at Full Scale First Flap Mode Frequencies, Including Rotor Frequency Response to Shaft Oscillations," NASA CR-114519, Oct. 1972.

[5]Peters, D. A. and Ormiston, R. A., "Flapping Response Characteristics of Hingeless Rotor Blades by a Generalized Harmonic Balance Method," NASA TN D-7856, 1975.

[6]Peters, D. A., "Hingeless Rotor Frequency Response with Unsteady Inflow," NASA SP-352, 1974, pp. 1-12.

[7]Hohenemser, K. H. and Yin, S.-K., "The Role of Rotor Impedance in the Vibration Analysis of Rotorcraft," *Vertica,* Vol. 3, No. 3, 1979, pp. 189-204.

[8]Yen, J. G. and McLarty, T. T., "Analysis of Rotor-Fuselage Coupling and Its Effect on Rotorcraft Stability and Response," *Vertica,* Vol. 3, No. 3, 1979, pp. 205-219.

[9]Warmbrodt, W. and Friedmann, P., "Formulation of Coupled Rotor/Fuselage Equations of Motion," *Vertica,* Vol. 3, No. 3, 1979, pp. 245-271.

[10]Kato, K. and Yamane, T., "A Calculation of Rotor Impedance for Hovering Articulated-Rotor Helicopters," *Journal of Aircraft,* Vol. 16, Jan. 1979, pp. 15-22.

[11]Kato, K. and Yamane, T., "Calculation of Rotor Impedance for Articulated Rotor Helicopters in Forward Flight," *Journal of Aircraft,* Vol. 16, July 1979, pp. 470-477.

[12]Kato, K. and Yamane, T., "Numerical Prediction of Typical Articulated Rotor Impedance," *Journal of Aircraft,* Vol. 16, July 1979, pp. 417-418.

[13]Loewy, R. G., "A Two-Dimensional Approximation to the Unsteady Aerodynamics of Rotary Wings," *Journal of Aeronautical Sciences,* Vol. 24, Feb. 1957, pp. 81-92.

[14]Anderson, W. D. and Watts, G. A., "Rotor Blade Wake Flutter—A Comparison of Theory and Experiment," *Journal of the American Helicopter Society,* Vol. 21, No. 2, April 1976, pp. 32-43.

[15]Friedmann, P. and Yuan, C., "Effect of Modified Aerodynamic Strip Theories on Rotor Blade Aeroelastic Stability," *AIAA Journal,* Vol. 15, July 1977, pp. 932-940.